Plume-driven subduction termination in 3-D mantle convection models

Erin Heilman[1,2] **and Thorsten W. Becker**[1,2,3]

[1]Institute for Geophysics, Jackson School of Geosciences, The University of Texas at Austin, Austin TX, USA

[2]Department of Earth and Planetary Sciences, Jackson School of Geosciences, The University of Texas at Austin, Austin TX, USA

[3]Oden Institute for Computational Sciences, The University of Texas at Austin, Austin TX, USA

Key Points:

- mantle plumes can terminate subduction in 3-D, damage rheology convection
- plumes can modulate subducting slabs and plate tectonic regimes
- plume-slab interactions are plausible contributions to the Karoo-Gondwana event

Corresponding author: Erin Heilman, `eheilman@lanl.gov`

Abstract

The effect of mantle plumes is secondary to that of subducting slabs for modern plate tectonics, e.g. when considering plate driving forces. However, the impact of plumes on tectonics and planetary surface evolution may nonetheless have been significant. We use numerical mantle convection models in a 3-D spherical chunk geometry with damage rheology to study some of the potential dynamics of plume-slab interactions. Substantiating our earlier work which was restricted to 2-D geometries, we observe a range of interesting plume dynamics, including plume-driven subduction terminations, even though the new models allow for more realistic flow. We explore such plume-slab interactions, including in terms of their geometry, frequency, and the overall effect of plumes on surface dynamics as a function of the fraction of internal to bottom heating. Some versions of such plume-slab interplay may be relevant for geologic events, e.g. for the inferred ∼183 Ma Karoo large igneous province formation and associated slab disruption. More recent examples may include the impingement of the Afar plume underneath Africa leading to disruption of the Hellenic slab, and the current complex structure imaged for the subduction of the Nazca plate under South America. Our results imply that plumes may play a significant role not just in kick-starting plate tectonics, but also in major modifications of slab-driven plate motions, including for the present-day mantle.

Plain Language Summary

Subduction of cold, strong lithospheric slabs is the main plate driving force within mantle convection. However, hot upwellings, mantle plumes, may have a greater role in modulating plate motions and slab trajectories than previously thought. We use 3-D numerical convection models that account for the weakening of rocks due to the accumulation of deformation to understand the effect that mantle plumes can have on subduction zones. We show that plumes can terminate subduction in a range of circumstances. We also test the effect of the amount of internal heating compared to heat from the core which is the major convective control on the importance of plumes. We discuss cases where these plume-slab terminations may have occurred on Earth, in the geological past, and for the present day through plate reconstructions and consideration of seismic tomography.

1 Introduction

Subduction of the cold, lithospheric boundary layer is the main driving force of plate tectonics through slab pull due to temperature-dependent viscosity and the dominance of internal heating in mantle convection. However, there is also feedback between subducting slabs and mantle plumes as long as there is some degree of bottom heating. While instabilities of the bottom thermal boundary layer can form plumes anywhere, a perturbation, for instance due to a subducting slab, will affect the timing and location for the formation of mantle plumes (e.g. Tan et al., 2002; Dannberg & Gassmöller, 2018; Arnould et al., 2020). This phenomenon suggests a possible feedback, or "talk-back", between plumes and slabs. Hence, when mantle plumes reach the top thermal boundary layer, i.e. the lithosphere, they too can perturb the cold thermal boundary layer, e.g. creating hotspot volcanics and large igneous provinces (LIPs), contributing to rifting and supercontinental breakup, subduction initiation, and contributing to a low viscosity asthenosphere (e.g. Koppers et al., 2021). When plumes reach the lithosphere at a subduction zone they can interact with slabs by temporarily speeding up plates (van Hinsbergen et al., 2011; Pusok & Stegman, 2020), affecting trench motion and convergence rates (Betts et al., 2012; Mériaux et al., 2015), being deflected by slabs (Druken et al., 2014; Kincaid et al., 2013), or disrupting slabs (Liu & Stegman, 2012; Heilman & Becker, 2022).

Such plume-slab disruption has been less well explored because one may expect a strong, thick slab to survive any plume-induced deformation. As a consequence, when discussing plume-slab interactions, most think of plumes as a possible driver to initiate subduction, and plume-affected plate tectonics has been explored in several models. Plumes may kick-start subduction either directly or by means of emplacing surface density contrasts (Ueda et al., 2008; Rey et al., 2014; Gerya et al., 2015; Baes et al., 2020), and plume induced modification of plate speeds may lead to far field forces for subduction initiation (van Hinsbergen et al., 2021).

However, if strain-dependent damage rheologies, e.g. akin to those explored by Gerya et al. (2021) implemented in simplified form following Fuchs and Becker (2021), are accounted for, plumes do in fact appear capable of terminating subduction as well (Heilman & Becker, 2022). This process can also be associated with an interesting feedback loop of subducting slabs initiating mantle plumes at the core–mantle boundary, plumes terminating subduction close to the surface after their ascent through the mantle, and the

broken-off slabs descending through the mantle to possibly begin the process again. While this would, of course, be just one aspect of the time-dependent convection system including possibly episodic or irregular plate tectonic motions, it is one interaction loop that leaves possibly diagnostic traces in rock record. For example, Fletcher and Wyman (2015) identified that in the past 60 Ma, 18 plumes have been within 1000 km of subduction zones, which points to plume-slab interactions, and potential terminations, as a relevant process to consider for the evolution of the plate tectonic system. Heilman and Becker (2022) explored the effects of internal heating, and thickness, or average temperature/age, of slabs as controlling factors for the likelihood of plumes terminating slabs and modifying the overall tectonic regime, such as a transition from plate-tectonics to stagnant lid. However, our earlier work was limited to 2-D, and one may rightly ask if such a restriction of flow is a precondition for plume-slab termination.

Investigating the nature of plume-slab termination in 3-D is both more realistic and more challenging. For the present-day mantle, we appear to mainly see plume-slab interactions where plumes are taking advantage of existing slab windows or tears, formed by plate reorganizations or local slab dynamics (Obrebski et al., 2010; Betts et al., 2012; Portner et al., 2017, 2020). Previously, Betts et al. (2012) showed based on 3-D modeling that a plume could modulate subduction in the case of trench rollback causing a subducting slab to move over a plume head. In this instance, a slab window was formed and subduction continued once the slab rolled completely over the plume head.

Investigations of suggested recent plume advance include the case of Canary toward the Alboran slab underneath the Atlas mountains (Duggen et al., 2009; Sun et al., 2014; Mériaux et al., 2015) and Afar toward Anatolia and the Hellenic subduction zone (Ershov & Nikishin, 2004; Faccenna et al., 2013; Hua et al., 2023). Present-day settings include the Yellowstone/Farallon case (Obrebski et al., 2010; Liu & Stegman, 2012) and the South American Juan de Fuca plume-slab window (Portner et al., 2017, 2020). These studies point to the lithosphere, e.g. in terms of slab tears or windows during trench rollback, or delamination, being the dominant control, and mantle plumes being secondary to lithosphere dynamics. Plume-slab termination in 3-D will depend on the lateral extents necessary for the interaction to cover, and thermo-mechanical heterogeneity of the mantle and crust. In particular, subduction termination can potentially become easier when damage rheologies or other tectonic inheritance leads to weakening of slabs, includ-

ing by segmentation and tears (van Hunen & van den Berg, 2008; Betts et al., 2012; Gerya et al., 2021).

Here, we model 3-D, mantle convection in a spherical "chunk" geometry with damage rheology and a mixed heating regime similar to Earth's convective vigor. We explore how damage rheology affects plume-slab interactions and show that plume-induced slab termination is indeed possible in 3-D. We discuss possible instances where this may have happened from the geologic record and present-day seismic tomography to relate our numerical models to the Earth.

2 Model Setup

To model mantle convection as a fluid convection problem in the infinite Prandtl number and incompressible, Boussinesq approximation, we can express conservation of momentum and mass as

$$-\nabla \cdot [2\eta\varepsilon\,(\mathbf{u})] + \nabla p = \rho\mathbf{g} = \rho_0\alpha(T - T_{ref}) \tag{1}$$

$$\nabla \cdot \mathbf{u} = 0, \tag{2}$$

and conservation of energy without shear heating as

$$\rho C_p \left(\frac{\partial T}{\partial t} + \mathbf{u}\cdot\nabla T\right) - \nabla \cdot k\nabla T = \rho H, \tag{3}$$

while allowing for advection of a compositional or general tracer field c

$$\frac{\partial c}{\partial t} + \mathbf{u}\cdot c = 0. \tag{4}$$

Here, ε is the strain-rate tensor, $\mathbf{u}$ velocity, p pressure, g gravity, T temperature, ρ density, with a reference of ρ_0 at T_{ref}, C_p specific heat capacity, k thermal conductivity, H the internal heat production, η viscosity, α thermal expansivity, and c composition. Eqs. (1) and (2) capture laminar Stokes flow, driven by thermal body forces, and eq. (3) describes the temperature field that is diffused and advected with the flow velocity $\mathbf{u}$, where the right-hand term is internal heat production. Eq. (4) governs how diffusion-free compositional fields evolve over time; in our models the compositional field tracked is a pas-

sive, effective "strain" property used to approximate damage evolution, as in Fuchs and Becker (2019, 2021), and does not involve additional, e.g., density contributions.

To solve eqs. (1-4), we use the open-source, finite element mantle convection code *ASPECT* (Kronbichler et al., 2012; Heister et al., 2017; Fraters et al., 2019). Our approach overall follows that of Heilman and Becker (2022), but we employ a Newtonian, Frank-Kamenetskii linearized temperature-dependent viscosity law (cf. Tackley, 2000a; Stein & Hansen, 2013) to simplify the model for a 3-D test case. The equation is as follows,

$$\eta\left(T\right) = \eta_{ref} \exp\left[\frac{E}{1+\frac{T}{T_{ref}}} - \frac{E}{2}\right] \tag{5}$$

where η_{ref} is a reference viscosity, E is a non-dimensional activation energy, and T_{ref} is a reference temperature. Added into this viscosity law is a viscosity jump at 660 km depth, where the η_{ref} is increased by a factor of 30 in the lower mantle, as expected from geoid modeling and slab sinking rates (e.g. Hager, 1984; Ricard et al., 1993; Steinberger & Calderwood, 2006).

Additionally, we include visco-plasticity and a simplified damage rheology in our models (e.g. Tackley, 2000b; Ogawa, 2003; Auth et al., 2003; Fuchs & Becker, 2019). *ASPECT* employs plasticity and a possible strain-weakening for modulating the yield stress (Glerum et al., 2018). When the viscous stress ($2\eta\dot{\varepsilon}_{II}$) exceeds the yield stress the viscosity is rescaled back to an effective yield viscosity (e.g., Moresi & Solomatov, 1998; Enns et al., 2005).

$$\eta_{eff} = \frac{\sigma_y}{2\dot{\varepsilon}_{II}}. \tag{6}$$

We then use a strain-based damage variable γ to reduce the yield stress from the background value (e.g. Lavier et al., 2000; Ogawa, 2003). Damage, γ, evolves according to

$$\frac{d\gamma}{dt} = \dot{\varepsilon}_{II} - \gamma\ A_d \cdot \exp\left[E_d\left(T - T_0\right)\right] \tag{7}$$

where $\dot{\varepsilon}_{II}$ is the second invariant of the strain-rate tensor, A_d is a timescale for strain-healing, E_d is a non-dimensional activation energy, following temperature- and time-dependent strain healing (Fuchs & Becker, 2019). Combining plasticity and such a damage rheology, which incorporates strain-weakening and strain-healing, can approximate the behavior of physical weakening processes like those inferred from grain-size dependent rhe-

170 **Table 1.** Model parameters

Parameter	Value
Temperature difference between thermal boundary layers	2373 K
Density ρ	3700 kg/m^3
Thermal expansivity α	$2 \cdot 10^{-5}$ K^{-1}
Thermal diffusivity κ	10^{-6} m^2/s
Specific heat capacity C	750 J/gK
Internal heating rate H	$5.0 \cdot 10^{-12}$ W/kg
Minimum viscosity η_{min}	10^{18} Pas
Maximum viscosity η_{max}	$2.5 \cdot 10^{24}$ Pas
Non-dimensional activation energy E	29.95
Reference viscosity η_{ref}	$4.5 \cdot 10^{19}$
Reference temperature for viscosity T_{ref}	2500 K
Yield stress for Damage Model	140 MPa
Minimum weakened yield stress for Damage Model	35 MPa
Yield stress for No Damage Model	55 MPa
Non-dimensional strain weakening factor s.w.f.	0.25
Non-dimensional activation energy for strain healing E_d	250
Non-dimensional timescale for strain healing A_d	10^{-7}

162 ologies (Fuchs & Becker, 2021), which is one of the suggested mechanisms for strain lo-
163 calization (e.g. Landuyt & Bercovici, 2009; Bercovici & Ricard, 2016). The strain-weakening
164 factor (Table 1) is set to reduce the yield stress linearly by 75%, i.e. from 140 to 35 MPa,
165 with parameters based on our earlier work. This accumulation/healing formulation al-
166 lows damage to persist and be advected in cold lithosphere while damage in the man-
167 tle is healed according to a specified rate with temperature (Table 1). We compare a model
168 with damage rheology to a model without to understand the effect of damage on the abil-
169 ity of mantle plumes to terminate subduction.

171 Temperature boundary conditions for our mixed heating convection model are 273 K
172 and 2573 K for the surface and core-mantle boundary, respectively, and the mechani-
173 cal boundary conditions are free slip on all sides. We use a reference internal heating value
174 of $5{\cdot}10^{-12}$ W/kg (Table 1) and compare the effect of different internal heating produc-
175 tion rates in subsequent models. The Earth's ratio of internal to bottom heating is in-
176 completely constrained and expected to be time-variable over planetary history because
177 of the decay of radiogenic material. We expect the balance of bottom to internal heat-
178 ing to control the relative importance of mantle plumes from a general understanding
179 of mantle convection (e.g. Davies, 1986; Zhong, 2006; Leng & Zhong, 2008; Foley & Becker,
180 2009) and our earlier, 2-D tests (Heilman & Becker, 2022).

We compare our reference model with a non-damage rheology case, which requires a lower yield stress to roughly match the convective vigor of the models with damage (cf. Fuchs & Becker, 2022). The effective Rayleigh number of our reference computation is $\sim 3.5{\cdot}10^6$. Bulk metrics such as surface heat flow are in Earth-like ranges (sec. 3.3), with surface velocities ∼3 times lower than for present-day plate speeds. We thus expect the dimensionalized model times to broadly correspond to actual time for our reference models. However, to make models with different parameters and hence convective vigor overall comparable, e.g., in terms of frequency of tectonic events, we also report times in units of overturn time, i.e. the typical time taken for a density anomaly to traverse the mantle and back. For the Earth, those can be converted by multiplying with relevant timescales, ∼300 Myr for ∼2 cm/yr average vertical motions.

3 Results

3.1 Damage Rheology Model

We first explore a model with the damage rheology and a yield stress of 140 MPa (Figure 1) building on the work by Heilman and Becker (2022). Including damage rheology in a convection model leads to potential localization of deformation, formation of persistent weak zones (e.g. Auth et al., 2003; Landuyt et al., 2008), as well as possibly an overall drop in bulk lithospheric strength, e.g. if damage reduces the yield stress (cf. Foley & Bercovici, 2014; Fuchs & Becker, 2019, 2022). In our models, the damage rheology weakens the subducting slabs and allows the weakness to persist because the slabs are cold. When mantle plumes strike the lithosphere, the damage is reduced as the plumes introduce heat. This can lead to the healing effect to take over, reducing the associated inherited weak zones on the surface. This does not mean that plumes make the lithosphere strong in our models, they still tend to decrease the viscosity of the lithosphere that they underplate, and generally lead to some mode of extension on the surface.

To visualize the plume-slab interactions and terminations we applied a temperature threshold for both the mantle plumes and subducting slabs. This thresholding allowed us to visualize features and interactions easily in 3-D. Figure 1a-h shows the temperature thresholding on the left for a plume-slab termination event. The total accumulated strain on the surface in Figure 1i-j shows the influence of the hot plume on the subduction zone in terms of damage. As the plume terminates subduction, the damage that

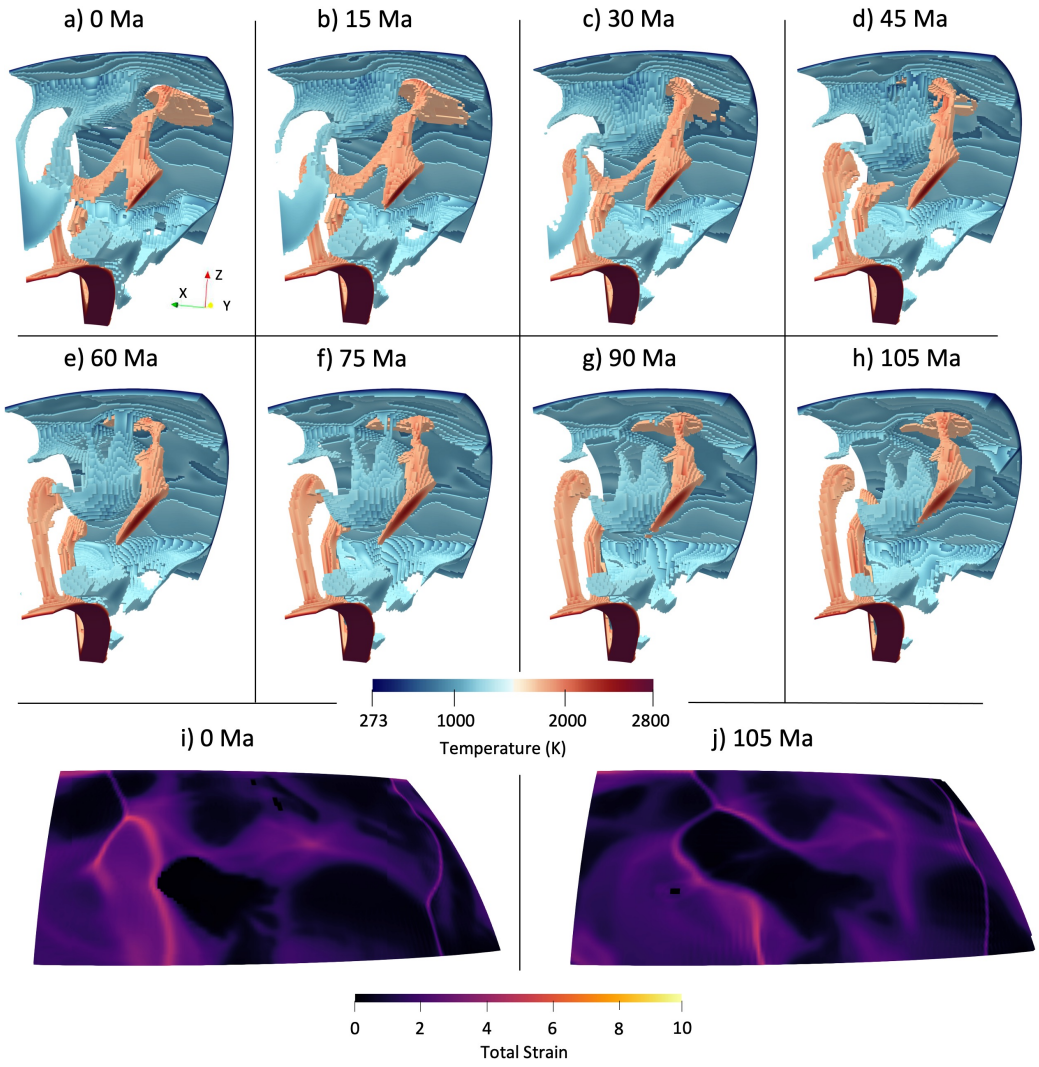

193 **Figure 1.** Example of a rising mantle plume terminating an subduction zone in 3-D for our
194 reference model with damage. a-h show temperature thresholds of plumes (∼1750-2773 K, red
195 colors) and slabs (273-∼1250 K, blue) over several timesteps showing a plume-slab interactions.
196 Plots i-j show the damage, expressed as effective "strain", at the surface at the first and last
197 timestep. When the plume strikes the surface, it resets the damage and it influences the subduc-
198 tion zone to bend around it.

was accumulated in the subduction zone in the lithosphere (Figure 1i) deflects around where the plume head strikes the lithosphere (Figure 1j), because the plume head introduces heat to the lithosphere which then increases the amount of strain healed above the plume. This configuration of damage remains frozen in the lithosphere and is advected along the surface until a new subduction zone is initiated from the damaged arc (cf. Foley & Bercovici, 2014; Fuchs & Becker, 2019; Heilman & Becker, 2022).

The reference model ran for a total of 3 model overturns, beginning from an initial steady state model run. During the qualifying model run time of 3 overturns, we observe 7 instances of plume-slab termination, i.e. an average of 2.3 terminations every overturn. In these models, termination of subduction is quantified through the temperature thresholding when no part of the subducting slab is connected to the trench of the subduction zone. These termination events do not tend to overlap in time, however we do observe an instance when two terminations are present at the same time. Terminations are clustered in time, with periods of quiescence, similar to what was observed and analyzed by Heilman and Becker (2022).

Six of the seven termination events occurred with a single plume impinging on a subduction zone causing the termination. The six events do vary in where the plume interacts with the slab along its lateral extent. If the plume strikes the center of the subducting slab, the termination tends to develop by creating a slab window that then extends along the length of the slab until it is fully terminated (as in Figure 1). If the plume head interacts with the slab closer to the subducting slabs lateral extent, then the termination has an unzipping effect as the slab begins detaching at the plume head and continues along the length of the slab. The last termination was caused by two plumes on both sides of the subduction zone that pinched out the subducting slab to shut off subduction.

Figures 2, 3, and 4 show these styles of termination in temperature, yield stress, strain rate, and total strain (accumulated damage) before and after termination, where termination is inferred from the visualization as the time when the slab is fully detached. We observe in these terminations that the subducting slab is strongly weakened during subduction, while the mantle plume is not further weakened by damage or plasticity, due to its inherent higher temperature (cf. Fuchs & Becker, 2019). Both the mantle plume and the subducting slab, in the area of the most bending in the slab, have high strain

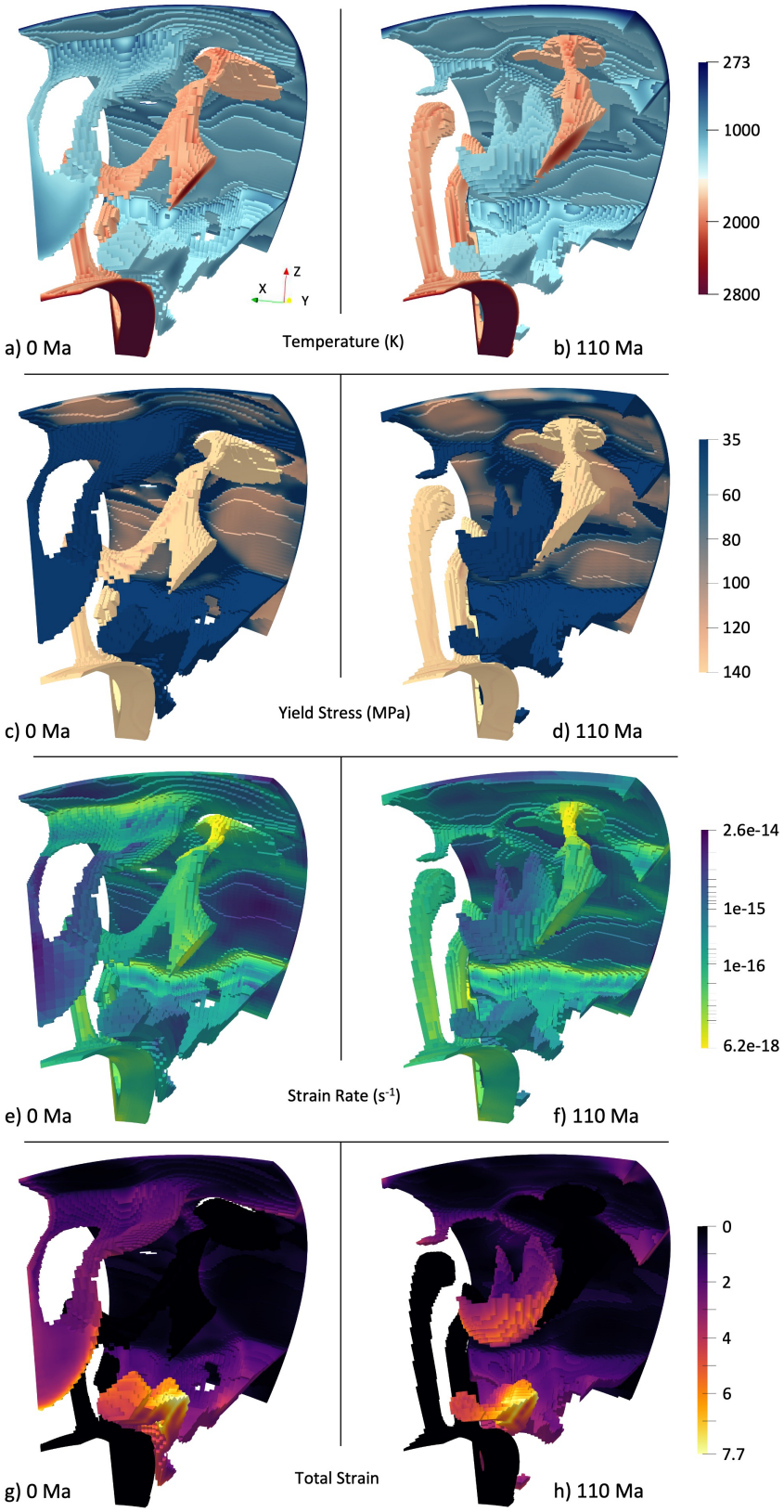

Figure 2. Temperature, yield stress, strain rate, and accumulated strain (damage) before (a, c, e, g) and after termination (b, d, f, h) for a typical termination (same termination as Figure 1) where a plume impinges on a subducting slab and shuts off subduction.

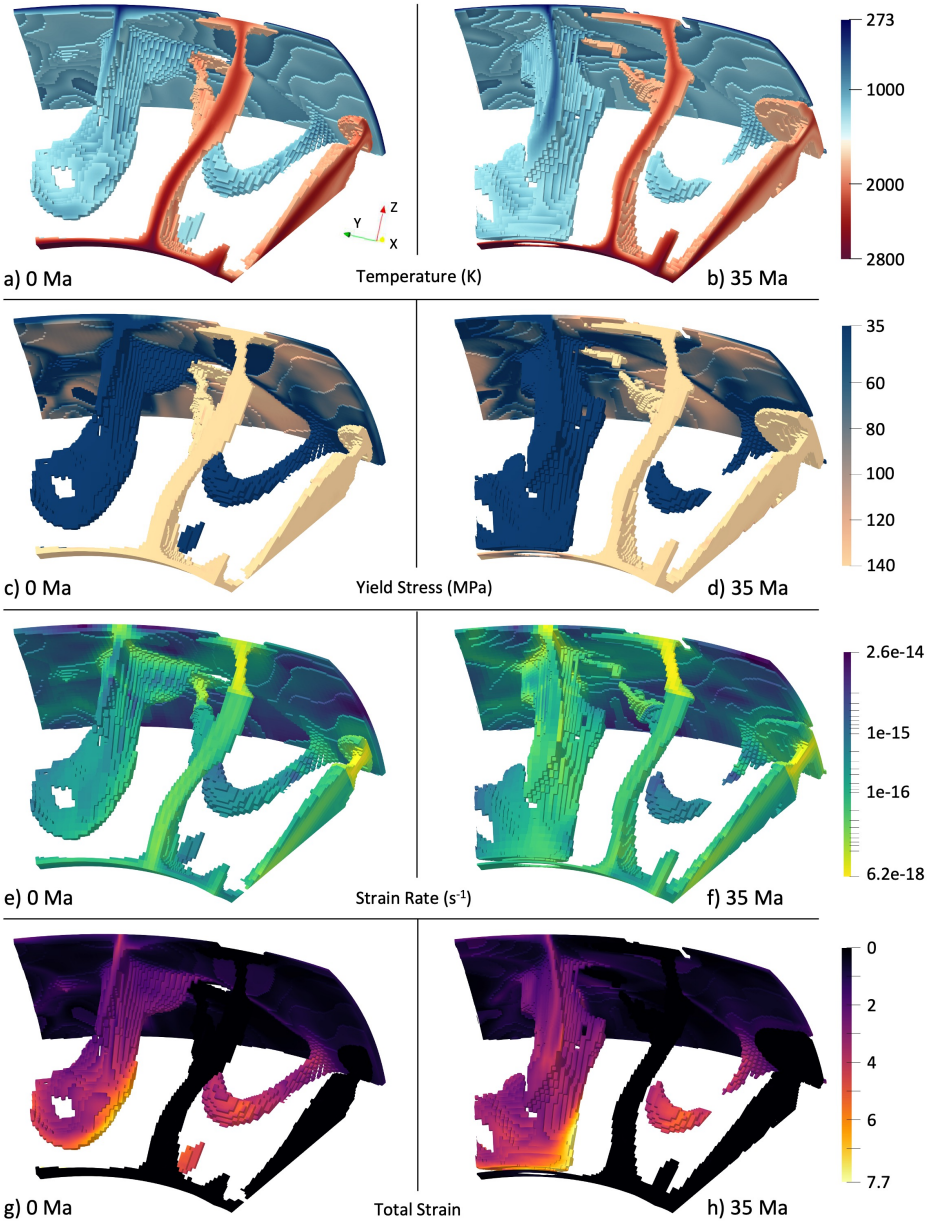

Figure 3. Temperature, yield stress, strain rate, and accumulated strain (damage) before (a, c, e, g) and after termination (b, d, f, h) for a termination where a plume impinges on the edge of a subducting slab and shuts off subduction by unzipping along the slab's length.

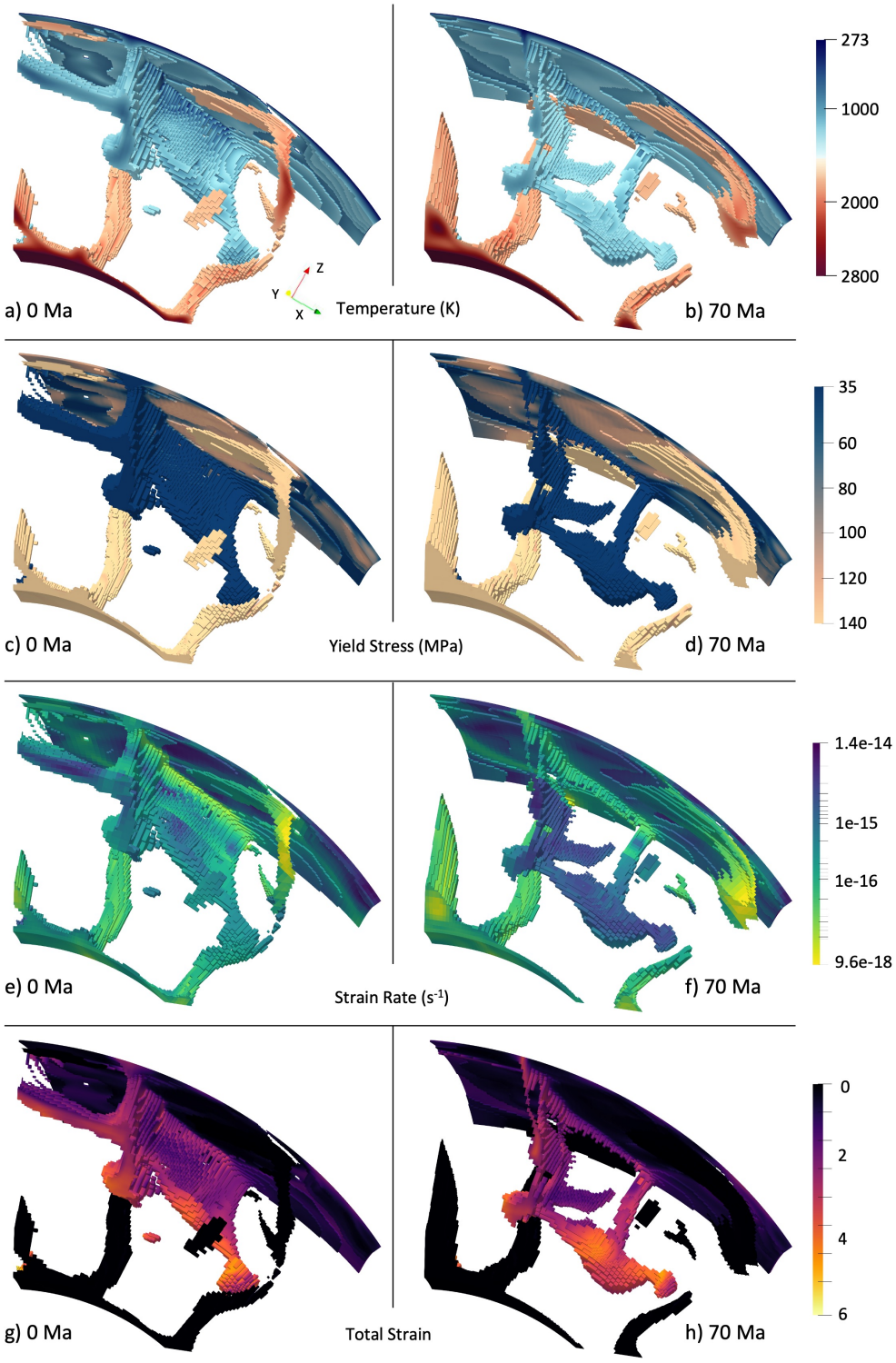

249 **Figure 4.** Temperature, yield stress, strain rate, and accumulated strain (damage) before (a,
250 c, e, g) and after termination (b, d, f, h) for a double-sided termination where two plumes pinch
251 out a subducting slab to shut off subduction.

rates that lessen after termination has occurred. In the case of damage, the subducting slabs have a moderate (∼2-5) amount of accumulated damage. This is a result of the weakening and slow healing in the cool slab, as opposed to the hot mantle plumes that have no accumulated damage. After termination occurs, the damage persists in the terminated slab as it sinks in the mantle, until the slab is heated enough that the damage is healed (cf. Fuchs & Becker, 2019).

However, as may be expected, and explored more fully in 2-D (Heilman & Becker, 2022), not every plume-slab interaction ends in a termination. We find at least five instances where a plume interacts with a subducting slab without causing a complete termination, i.e. a roughly 60% chance of plumes shutting down subduction if they get close to slabs, for our chosen parameter values. Some of these plume-slab interactions result in no change to the subducting slab morphology from the plume. While in some cases, the plume creates a slab window in the subducting slab but subduction is able to continue normally, as has been suggested for modern settings based on seismic tomography.

3.2 Non-Damage Rheology Model

We include a model without the damage rheology to compare to the plume-slab interactions we observe in the damage model. In this non-damage model, the background yield stress has to be lowered to 55 MPa from 140 MPa to achieve the same convective vigor and maintain a mobile convective regime (comparable Rayleigh number of $\sim 3.8 \cdot 10^6$). Both of the used yield stress values are required to achieve plate-like motions with a mobile lid in our models, however, the values are much smaller than what would be expected from rock mechanics. This is a typical finding for visco-plastic, plate-like convection models (e.g. Moresi & Solomatov, 1998; van Heck & Tackley, 2008; Foley & Becker, 2009), and might indicate some additional weakening mechanism, such as hydration. However, our point here is not about the absolute values, but we merely provide an attempt to compare damage and no-damage cases at similar convective vigor and tectonic style.

Our non-damage model has a total run time of ∼6 overturns, and this model showed only one example of plume-slab termination. In this termination, a plume first formed a slab window in a subducting slab, which then caused a slab tear on either side of the slab window, and lead to the eventual termination of the subduction zone. There were four other instances where a mantle plume caused the formation of a slab window that

did not result in an immediate termination of subduction. In this non-damage rheology case, the yield stress in the subducting slab can be higher than that in the damage rheology case due to the lack of weakening. This higher slab yield stress is likely why we see more formations of slab windows than full plume-slab terminations in our non-damage model.

3.3 Ratios of Internal Heating

We expect the amount of internal heating to affect the importance of plumes, which are trivially absent if there is no bottom heating, and whose effect will be maximal for pure bottom heating. To compare our reference damage rheology results, two other models were run with a lower ($5 \cdot 10^{-13}$ W/kg) and a higher ($2 \cdot 10^{-11}$ W/kg) amount of internal heat production, i.e. 0.1 and 4 times the heat production of the initial damage rheology model. The heat flow time series for the three models are shown in Figure 5. The average heat flow for the reference model (Figure 5a) is 1.81 TW for the core-mantle boundary (CMB) and 4.69 TW for the surface. The relative contribution of 61.5% from internal heating for the reference model is in the ballpark of estimates for the Earth's mantle (Leng & Zhong, 2008; Lay et al., 2008; Jaupart et al., 2015), which are, however, uncertain. The average heat flow for the lower heating model (Figure 5b) is 1.67 TW out of the CMB and 3.77 TW out of the surface, for 55% contribution from internal heating. The average heat flow for the higher heating model (Figure 5c) is 1.76 TW out of the CMB and 7.27 TW out of the surface, for 75% contribution from internal heating.

Considering absolute values, our 3-D spherical chunk is roughly 15% of the surface area of the Earth. Scaling the heat flow out of the surface of the model to Earth would be roughly 31.3 TW for the reference model, and 25.1 TW and 48.5 TW for the lower and higher heating model, respectively. These values are comparable to estimates for the convective heat flow of the mantle, ∼38 TW (Jaupart et al., 2015). This implies that while our focus here is, of course, mainly to explore the general controls on plume dynamics, and we did not account for secular cooling, the overall convective vigor of the models may be comparable to the mantle.

While having only changed the internal heat production, complexities arise because different average viscosities result via the temperature-dependent creep laws used. This means that these models have different Rayleigh numbers, or convective vigor, with es-

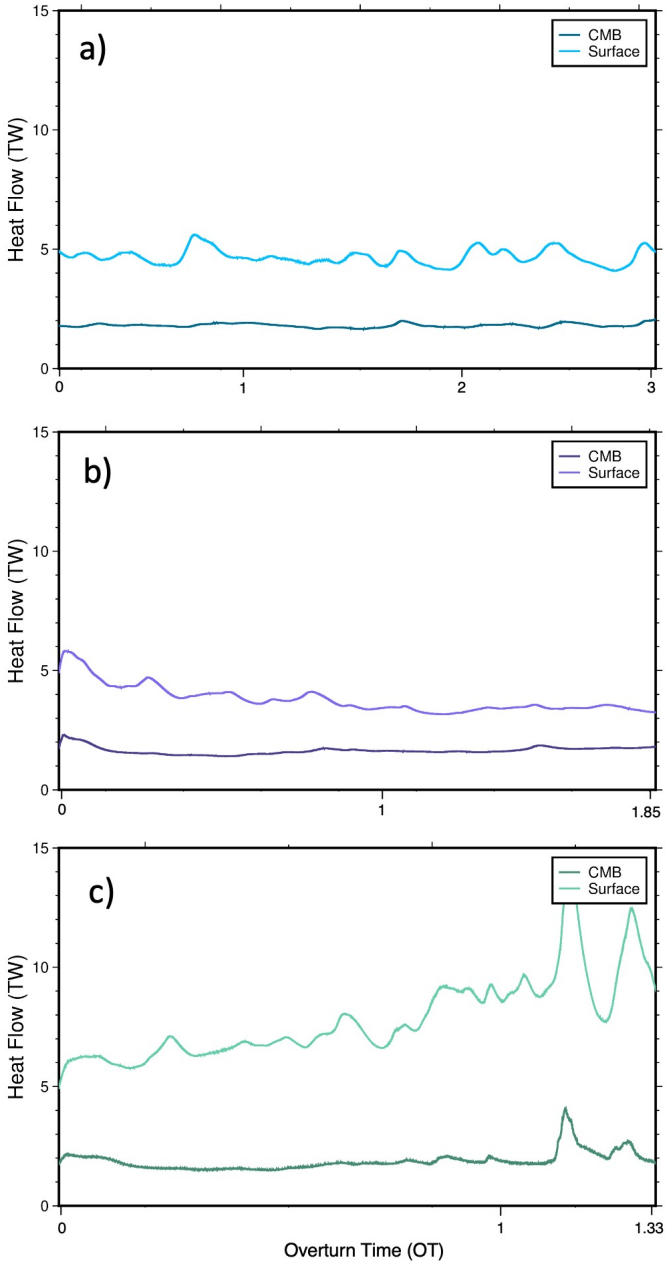

318 **Figure 5.** Heat flow out of the CMB and surface are plotted over overturn times for three
319 models. a) Damage Model. b) Lower Internal Heating Model. c) Higher Internal Heating Model.

timates for the Rayleigh numbers $4.65 \cdot 10^5$, $9.95 \cdot 10^6$, and $7.16 \cdot 10^7$ for the lower, reference, and higher heating cases, respectively. This changing convective vigor does have an effect on the planform of convection. However, these models all remain predominantly mobile and in a plate tectonic-like convection regime, meaning they should be broadly comparable in terms of their dynamics, including plume-slab interactions.

The model with a lower proportion of heating ran for a total of 1.85 overturns from an initial steady state model. This model showed eleven plume-slab terminations, i.e. roughly 5 per overturn. These terminations follow the same trend as in the reference model, where the subducting slab is fully weakened before the termination, strain rate is high in both the slab and plume and lessens after termination, and the subducting slab is damaged prior to termination. We also see in this model a non-termination event creating a slab window in the subducting slab and subduction continues. Specifics of these interactions and the detailed numbers of terminations per a given typical model time are, of course, subject to stochastic fluctuations.

The model with a higher proportion of heating had a total run time of 1.33 overturns after starting from an initial steady state model. This model showed two plume-slab terminations, i.e. $\sim$1.5 terminations per one overturn. This model had hotter average mantle temperatures (2034 K compared to the reference model 1518 K) and therefore hotter subducting slab temperatures due to the increased proportion of internal heating. It was more difficult to identify instances when plumes were actively shutting off subduction as the hotter mantle led to the subducting slabs warming quickly and detaching even without plume influence. The model becomes unstable towards the end of its run time and moves into an episodic regime (as seen in Figure 5c) and may be more relevant for ealy Earth rather than, say, Cenozoic mantle convection (e.g. van Hunen & van den Berg, 2008).

Given variations in the relative importance of bottom and internal heating, we thus find the expected effect on the rate of plume-slab terminations per overturns. All models show plume-slab terminations and interactions, but for the lower internal heating model the frequency of plume-termination events was almost double the reference model. The opposite is true for the higher internal heating model with fewer plume driven subduction terminations, substantiating the 2-D results of Heilman and Becker (2022). We also ran two other models with intermediate heat production of $8{\cdot}10^{-12}$ W/kg and $1{\cdot}10^{-11}$ W/kg

for validation and the termination numbers were in between the higher heat model and the reference model.

Due to the additional degrees of freedom provided by 3-D flow compared to the analysis of Heilman and Becker (2022), and the highly time-dependent nature of the convective system, further, systematic analysis of controlling factors beyond the overall effect of internal heating has to be somewhat limited. We measured internal slab temperature for both terminating and non-terminating plume-slab interactions by sampling temperatures from the subducting slab for a period of 60 Ma (well within the overall termination and interaction times). The temperatures were collected over a 50 km section of the subduction zone where the plume was actively interacting with it, at a spacing of 10 km intervals. These data were averaged over the length (50 km) and the standard deviation was taken to show the variability of temperature within the slab. In general, we find that the non-terminating interactions are typically happening for slabs that are colder and hence thicker, as expected (Heilman & Becker, 2022).

We plot slab temperatures for terminations and non-terminations as a function of internal heating in Figure 6. As the average mantle temperature increases, plumes contribute less to the convective dynamics, so there are less terminations overall. For these models, the respective average mantle temperatures are 1278, 1518, and 2034 K. The age of thickness of the subducting slab as reflected in our temperature estimates during non-terminations follows this trend as well, shown most clearly in Figure 6c where the non-termination temperatures increase with the proportion of internal heating.

4 Discussion

Our models show that plume-driven subduction terminations occur in 3-D spherical geometry convection models, substantiating the suggestion of Heilman and Becker (2022). This implies that plume-induced subduction termination may indeed happen on Earth, if convective vigor and actual rock rheology are similar to those represented by our model. A prerequisite for termination is that the slab can be weakened, as is the case for our damage rheology model. While slab pull forces can be supported for plate-like motions even in the presence of weakening (cf. Gerya et al., 2021), the accumulated damage makes it easier for the mantle plume to cut through, or pinch out, the subducting slab (Figures 2, 3, and 4). While it is perhaps becoming more broadly accepted that the

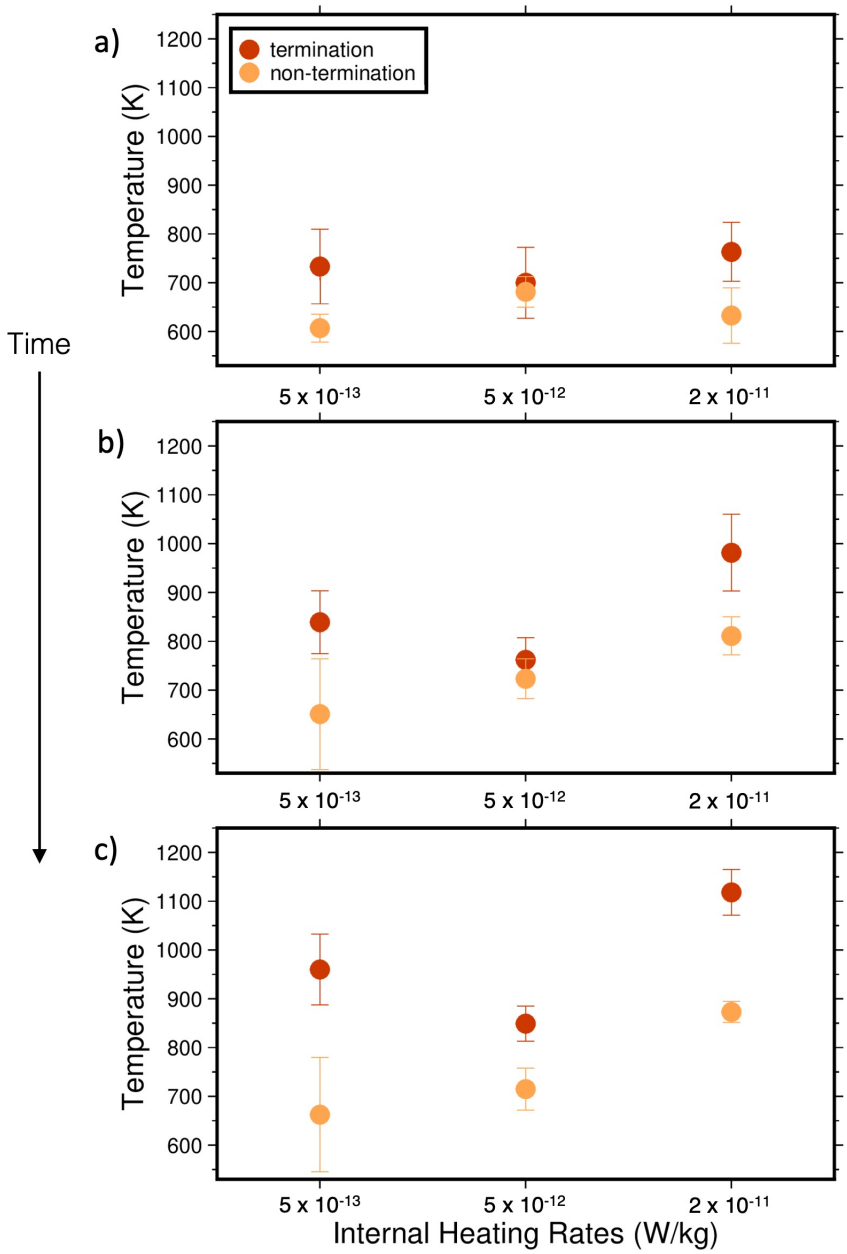

Figure 6. Subducting slab temperatures for terminations and non-terminations for each ratio of internal heating. Plots a), b), and c) increase in 20 Ma time increments showing the trend in slab temperature over time for each internal heating ratio.

lithosphere is significantly weakened in the trench region where the plate is bending, our rheological choices may, of course, lead to slabs that are weaker than in the Earth's mantle. However, since slab segmentation is a widely inferred process (e.g. Tan et al., 2002; Liu & Stegman, 2012), we would expect plume-slab terminations for stronger slabs to be perhaps less frequent on Earth than in our models, rather than being completely absent.

Besides rheology, the other control on the importance of plume-slab interactions is the degree of bottom to internal heating. Our results for a higher to lower rate of internal heating (sec. 3.3 and Figure 6) could be interpreted as being indicative of the evolution of mantle dynamics from the early Earth to present-day. As the internal heating of the mantle has decreased by a factor of $\sim$4 over time with an effective decay timescale of $\sim$3 Ga (e.g. Jaupart et al., 2015) due to the half life of radiogenic elements, there will be a greater effect of mantle plumes during the more recent periods of plate tectonics, including relatively more frequent plume-induced subduction terminations. Such effects due to active upwellings may add to the possible contributions of accumulating damage and persistent sutures in the lithosphere to make plate tectonics more time-dependent toward the present, even though the overall convective vigor may decrease with progressive cooling (Foley & Bercovici, 2014; Fuchs & Becker, 2022).

As our models are freely convecting, rather than being tailored to specific tectonic scenarios, we can only make observations about what sorts of subduction zones get terminated and what the typical geometry and dynamics of those cases are. The main scenarios we observe are a plume head impinging either in front or behind the subducting slab to cause termination (Figures 2 and 3) and plumes on either side of a subducting slab pinching out a subduction zone leading to termination (Figure 4). The first example is most common in the model, occurring $\sim$85% of the time in the reference, damage-rheology model, and it is the only mode in the non-damage rheology, lower internal heating, and higher internal heating cases. Typically, this process begins as a plume initiating a slab window in the subducting slab. The plume can then either remain stationary with the subduction zone and the termination happens in the plume's presence, or the plume may advect or diffuse away from the subducting slab, but the influx of heat from the plume was enough to cause the termination. The second scenario has two plumes pinching out a subduction zone to cause a termination. We see this type of termination

less frequently in our models, and this scenario is perhaps also less likely on Earth as it requires plumes on either side of a subduction zone.

To discuss disruption frequency of terminations, we must scale back to dimensional Earth time. Thus, we use 300 Myr as an appropriate comparison of overturn time to dimensional time for Cenozoic mantle convection. The disruption frequency of terminations is then one termination every 50 Myr for the lower heating model, every 130 Myr for the reference model, and every 200 Myr for the higher heating model. Additionally, the non-damage model frequency with its one termination would be every 1.8 billion years. This scaling of frequency correlates with the proportion of internal heating of the models, with the most frequent occurring in the model with the highest proportion of bottom heating and becoming less frequent with higher proportions of internal heating. This frequency suggests there may be several examples of this plume-slab termination in Earth's history.

4.1 Comparison to past and modern-day tectonic settings

Plume-slab terminations show interesting dynamics in geodynamic models, but there is also some indication of their existence in past and present-day geology. One example during the Jurassic (201-145 Ma) is related to the Karoo-Ferrar LIP eruption in southwestern Gondwana. While it is generally agreed that there was a time of flat slab subduction previous to the LIP emplacement, there is debate as to how this flat slab subduction ended (Dalziel et al., 2000; Luttinen, 2018; Navarrete et al., 2019; Ruhl et al., 2022). Figure 7 shows our interpretation in 3-D of the dynamics of this system, motivated by our 3-D model dynamics. If the rising mantle plume was responsible for flat slab subduction (Dalziel et al., 2000), it may have subsequently broke through the slab, reached the lithosphere, and created the Karoo-Ferrar LIP. This scenario can also explain the bilateral geochemical sourcing of the Karoo from both deep mantle sources and subduction-modified upper mantle sources as the plume rises and terminates. The subducting slab could have then unzipped from where the mantle plume broke through, explaining the subduction-influenced upper mantle signature in the Ferrar LIP (Luttinen, 2018).

A more recent example of plume-slab dynamics is the Arabian-Anatolian-Aegean system (Ershov & Nikishin, 2004; Faccenna et al., 2013; Hua et al., 2023). Subduction

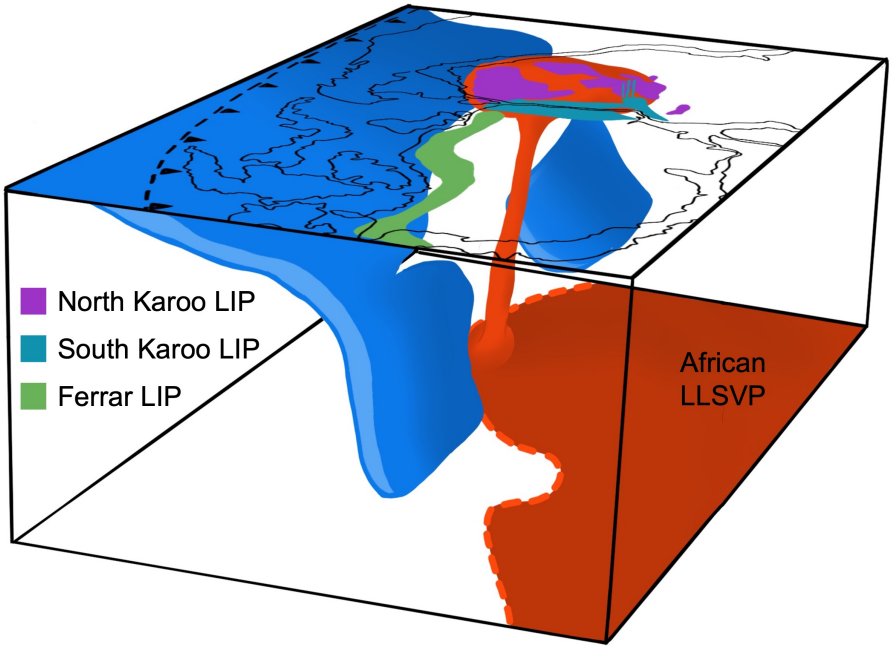

Figure 7. 3-D reconstruction of southwestern Gondwana during the Jurassic showing on the surface the emplacement of LIPs (Luttinen, 2018). Rendering in the mantle shows projected African LLSVP, mantle plume that cutoff subduction underneath southwestern Gondwana and shows propagation of slab shutoff.

in the Mediterranean has been inferred to have been active 30 million years ago as the Afar plume was upwelling under the Arabian plate to the southeast (cf. Faccenna et al., 2013). Volcanic ages and other constraints have been interpreted such that the plume then moved northward toward Anatolia, and that this plume advance was driven or at least assisted by mantle flow, including via a fragmentation of the Mediterranean slab. The formation of a slab gap underneath Anatolia leading to the current Hellenic segment of the trench might have led to asthenospheric suction and contributed to Afar plume advance (Faccenna et al., 2013; Hua et al., 2023). Our results here, and the 2-D models of Heilman and Becker (2022), suggest that the Afar plume may have, in fact, played a more active role in partitioning subduction along the northern margin of Africa.

For the modern-day, the Nazca-South American subduction zone may serve as an example for the effect of plumes on slabs. Based on interpretation of seismic tomography, Portner et al. (2017, 2020) suggested that the Juan de Fuca plume was taking advantage of a previously created slab window. With our model findings, we can speculate that this interaction is the beginning of a plume-slab termination where a slab window is developed first and a few million years later leads to subduction shutoff. In Figure 8, we interpret the tomography of Portner et al. (2020) for the Nazca slab and mantle. In this figure the dotted lines are interpretations of the lateral extent of the plume and slab. The mantle plume may have modified and broken through part of the subducting slab. This stage of a plume lying under a subducting slab and creating a slab window is very similar to the beginning stages of several terminations that we observe in our model (i.e. Figure 1). In the future, this interaction may turn into a termination if the slab is sufficiently affected by the presence of the plume.

Relevant plume-slab interactions may also be present in other areas for the modern-day, including on the western side of the Pacific where a range of hot anomalies have been imaged in proximity to possibly fragmented slabs (e.g. Obayashi et al., 2009; Tao et al., 2018), and the effects of hot mantle anomalies on subduction have been modeled (e.g. Morishige et al., 2010). Plume-slab interactions in east Asia have been postulated for origin of the Changbaishan volcanic complex, where intraplate volcanism may be driven by a plume disrupting or at least affecting the subducting Pacific plate (Tang et al., 2014). Seismic imaging has been interpreted to show hot material from the deep mantle rising through a gap in the subducting slab (Tang et al., 2014), a type of interaction between plumes and slabs consistent with our model findings.

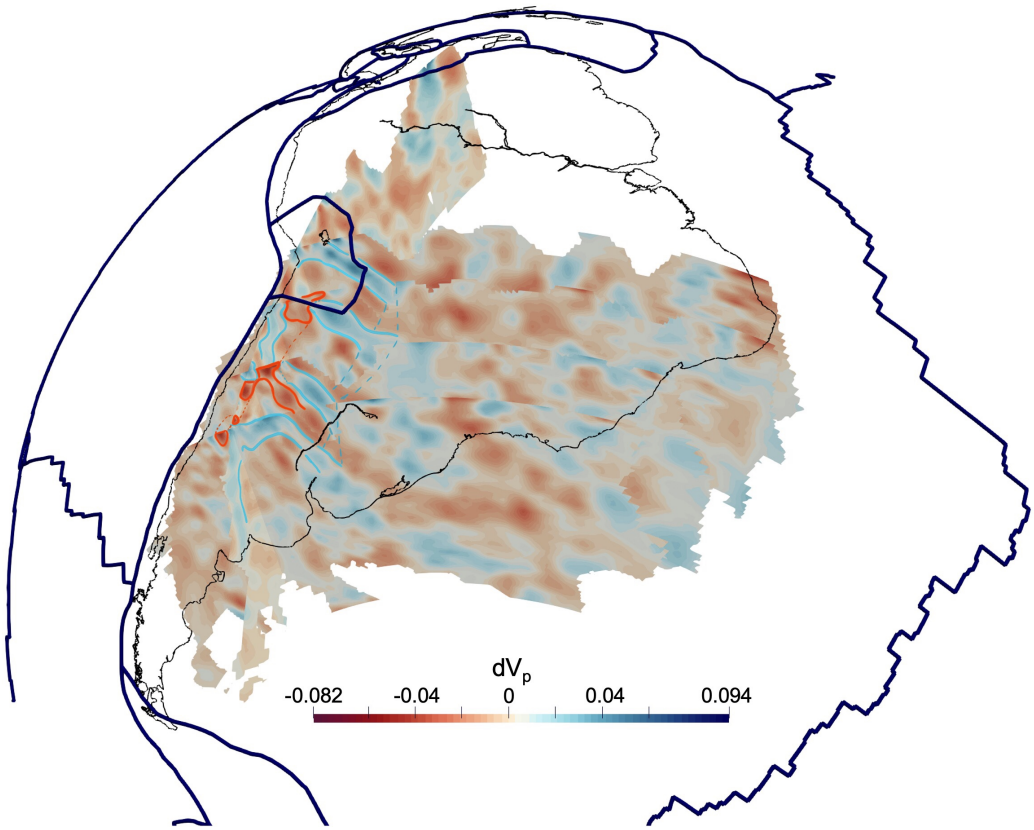

Figure 8. Tomography fence diagram of southern South America using dV_p using tomographic data from Portner et al. (2020). Interpretation of 3D plume-slab interaction structure is overlain in blue for subducting slab and red for mantle plume. South America is outlined in black while tectonic plates are outlined in dark blue.

5 Conclusions

We find that plume-induced subduction terminations occurs in 3-D, spherical geometry mantle convection models. Terminations are found throughout our models, but more likely in cases with damage rheology. A single plume can directly shut off subduction by puncturing and cutting off a slab from below, two plumes can pinch out subduction from the side, and a single plume can cause an lateral unzipping of a descending slab. Natural examples where these processes may help explain the thermo-chemical evolution of the continental lithosphere include the Karro-Ferrar LIP, the Afar-Anatolia Agean system, and present-day settings in the western and eastern Pacific subduction systems. Plume-slab termination frequency is inversely related to the proportion of internal heating, implying that plume-slab interactions may have become more prevalent over planetary evolution. Our models can contribute to a better understanding of the relationship between subducting slabs and rising mantle plumes and the effect and expressions of slab-plume "talk-back" in the evolution of the plate tectonic system.

6 Open Research

ASPECT is an open-source mantle convection code hosted by the Computational Infrastructure for Geodynamics, all features used are available in ASPECT version 2.4.0-pre (at `aspect.geodynamics.org/`), which is available at `doi.org/10.5281/zenodo.6903424`. The necessary parameter files to replicate models can be found at `doi.org/10.5281/zenodo.8102543`.

Acknowledgments

This project was funded by the National Science Foundation under award EAR-1853856. We thank the developers and the Computational Infrastructure for Geodynamics (geodynamics.org) which is funded by the National Science Foundation under award EAR-0949446 and EAR-1550901 for supporting the development of ASPECT. We also thank Portner et al. (2020) for making their tomographic model available freely, and J. Dannberg and C. Faccenna for providing comments on a thesis chapter which formed the basis for this manuscript.

References

Arnould, M., Coltice, N., Flament, N., & Mallard, C. (2020). Plate tectonics and mantle controls on plume dynamics. *Earth Planet. Sci. Lett.*, *547*, 116439.

Auth, C., Bercovici, D., & Christensen, U. R. (2003). Two-dimensional convection with a self-lubricating, simple-damage rheology. *Geophys. J. Int.*, *154*, 783–800.

Baes, M., Sobolev, S., Gerya, T., & Brune, S. (2020). Plume-induced subduction initiation: Single-slab or multi-slab subduction? *Geochem., Geophys., Geosys.*, *21*(2), e2019GC008663.

Bercovici, D., & Ricard, Y. (2016). Grain-damage hysteresis and plate tectonic states. *Phys. Earth Planet. Inter.*, *253*, 31–47.

Betts, P. G., Mason, W. G., & Moresi, L. (2012). The influence of a mantle plume head on the dynamics of a retreating subduction zone. *Geology*, *40*(8), 739-742.

Dalziel, I. W., Lawver, L., & Murphy, J. (2000). Plumes, orogenesis, and supercontinental fragmentation. *Earth and Planetary Science Letters*, *178*(1-2), 1–11.

Dannberg, J., & Gassmöller, R. (2018). Chemical trends in ocean islands explained by plume–slab interaction. *Pro. Nat. Acad. Sci.*, *115*, 4351–4356.

Davies, G. F. (1986). Mantle convection under simulated plates: effects of heating modes and ridge and trench migration, and implications for the core-mantle boundary, bathymetry, the geoid and Benioff zones. *Geophys. J. R. Astr. Soc.*, *84*, 153–183.

Druken, K., Kincaid, C., Griffiths, R., Stegman, D., & Hart, S. (2014). Plume–slab interaction: the Samoa–Tonga system. *Phys. Earth Planet. Inter.*, *232*, 1–14.

Duggen, S., Hoernle, K., Hauff, F., Klügel, A., Bouabdellah, M., & Thirlwall, M. F. (2009). Flow of Canary mantle plume material through a subcontinental lithospheric corridor beneath Africa to the Mediterranean. *Geology*, *37*, 283—286.

Enns, A., Becker, T. W., & Schmeling, H. (2005). The dynamics of subduction and trench migration for viscosity stratification. *Geophys. J. Int.*, *160*, 761–775.

Ershov, A., & Nikishin, A. (2004). Recent geodynamics of the Caucasus-Arabia-east Africa region. *Geotectonics*, *38*, 123–136.

Faccenna, C., Becker, T. W., Jolivet, L., & Keskin, M. (2013). Mantle convection in the Middle East: Reconciling Afar upwelling, Arabia indentation and Aegean

554 trench rollback. *Earth Planet. Sci. Lett.*, *375*, 254–269.

555 Fletcher, M., & Wyman, D. A. (2015). Mantle plume-subduction zone interactions
556 over the past 60 Ma. *Lithos*, *233*, 162-173.

557 Foley, B. J., & Becker, T. W. (2009). Generation of plate tectonics and mantle
558 heterogeneity from a spherical, visco-plastic convection model. *Geochem., Geo-*
559 *phys., Geosys.*, *10*(Q08001). doi: 10.1029/2009GC002378

560 Foley, B. J., & Bercovici, D. (2014). Scaling laws for convection with temperature-
561 dependent viscosity and grain-damage. *Geophys. J. Int.*, *199*, 580–603.

562 Fraters, M. R. T., Bangerth, W., Thieulot, C., Glerum, A. C., & Spakman, W.
563 (2019). Efficient and practical Newton solvers for nonlinear Stokes systems in
564 geodynamics problems. *Geophys. J. Int.*, *218*, 873–894.

565 Fuchs, L., & Becker, T. W. (2019). Role of strain-dependent weakening memory on
566 the style of mantle convection and plate boundary stability. *Geophys. J. Int.*,
567 *218*, 601–618.

568 Fuchs, L., & Becker, T. W. (2021). Deformation memory in the lithosphere: A com-
569 parison of damage-dependent weakening and grain-size sensitive rheologies. *J.*
570 *Geophys. Res.*, *126*, e2020JB020335.

571 Fuchs, L., & Becker, T. W. (2022). On the role of rheological memory
572 for convection-driven plate reorganizations. *Geophys. Res. Lett.*, *49*,
573 e2022GL099574.

574 Gerya, T. V., Bercovici, D., & Becker, T. (2021). Dynamic slab segmentation due to
575 brittle-ductile damage in the outer rise. *Nature*, *599*, 245–250.

576 Gerya, T. V., Stern, R. J., Baes, M., Sobolev, S. V., & Whattam, S. A. (2015).
577 Plate tectonics on the Earth triggered by plume-induced subduction initiation.
578 *Nature*, *527*(7577), 221–225.

579 Glerum, A., Thieulot, C., Fraters, M., Blom, C., & Spakman, W. (2018). Nonlinear
580 viscoplasticity in ASPECT: benchmarking and applications to subduction.
581 *Solid Earth*, *9*, 267–294.

582 Hager, B. H. (1984). Subducted slabs and the geoid: constraints on mantle rheology
583 and flow. *J. Geophys. Res.*, *89*, 6003–6015.

584 Heilman, E., & Becker, T. W. (2022). Plume-slab interactions can shut off subduc-
585 tion. *Geophysical Research Letters*, *49*, e2022GL099286.

586 Heister, T., Dannberg, J., Gassmöller, R., & Bangerth, W. (2017). High accuracy

mantle convection simulation through modern numerical methods – II: realistic models and problems. *Geophys. J. Int.*, *210*, 833–851.

Hua, J., Fischer, K., Gazel, E., Parmentier, E., & Hirth, G. (2023). Long-distance asthenospheric transport of plume-influenced mantle from Afar to Anatolia. *Geochem., Geophys., Geosys.*, *24*, e2022GC010605.

Jaupart, C., Labrosse, S., Lucazeau, F., & Marechal, J.-C. (2015). Temperatures, heat and energy in the mantle of the Earth. In G. Schubert (Ed.), *Treatise on geophysics* (2nd ed., pp. 223–270). Elsevier.

Kincaid, C., Druken, K., Griffiths, R. W., & Stegman, D. R. (2013). Bifurcation of the Yellowstone plume driven by subduction-induced mantle flow. *Nature Geosc.*, *6*, 395–399.

Koppers, A. A., Becker, T. W., Jackson, M. G., Konrad, K., Müller, R. D., Romanowicz, B., ... Whittaker, J. M. (2021). Mantle plumes and their role in earth processes. *Nature Rev. Earth & Environ.*, *2*, 382–401.

Kronbichler, M., Heister, T., & Bangerth, W. (2012). High accuracy mantle convection simulation through modern numerical methods. *Geophys. J. Int.*, *191*, 12–29.

Landuyt, W., & Bercovici, D. (2009). Formation and structure of lithospheric shear zones with damage. *Phys. Earth Planet. Inter.*, *175*(115–126).

Landuyt, W., Bercovici, D., & Ricard, Y. (2008). Plate generation and two-phase damage theory in a model of mantle convection. *Geophys. J. Int.*, *174*, 1065–1080.

Lavier, L. L., Buck, W. R., & Poliakov, A. N. B. (2000). Factors controlling normal fault offset in an ideal brittle layer. *J. Geophys. Res.*, *105*, 23431—23442.

Lay, T., Hernlund, J., & Buffett, B. (2008). Core-mantle boundary heat flow. *Nature Geosc.*, *1*, 25–32.

Leng, W., & Zhong, S. (2008). Controls on plume heat flux and plume excess temperature. *J. Geophys. Res.*, *113*.

Liu, L., & Stegman, D. R. (2012). Origin of Columbia River flood basalt controlled by propagating rupture of the Farallon slab. *Nature*, *482*, 386–389.

Luttinen, A. V. (2018). Bilateral geochemical asymmetry in the Karoo Large Igneous Province. *Scientific Reports*, *8*, 5223.

Mériaux, C., Duarte, J. C., Schellart, W. P., & Mériaux, A.-S. (2015). A two-way

620 interaction between the Hainan plume and the Manila subduction zone. *Geo-*
621 *phys. Res. Lett.*, *42*, 5796–5802. doi: 10.1002/2015GL064313

622 Moresi, L. N., & Solomatov, V. (1998). Mantle convection with a brittle lithosphere:
623 thoughts on the global tectonic styles of the Earth and Venus. *Geophys. J.*
624 *Int.*, *133*, 669–682.

625 Morishige, M., Honda, S., & Yoshida, M. (2010). Possibility of hot anomaly in
626 the sub-slab mantle as an origin of low seismic velocity anomaly under the
627 subducting Pacific plate. *Phys. Earth Planet. Inter.*, *183*, 353–365.

628 Navarrete, C., Gianni, G., Encinas, A., Márquez, M., Kamerbeek, Y., Valle, M.,
629 & Folguera, A. (2019). Triassic to Middle Jurassic geodynamic evolution of
630 southwestern Gondwana: From a large flat-slab to mantle plume suction in a
631 rollback subduction setting. *Earth-Science Reviews*, *194*, 125–159.

632 Obayashi, M., Yoshimitsu, J., & Fukao, Y. (2009). Tearing of stagnant slab. *Science*,
633 *324*, 1173–1175.

634 Obrebski, M., Allen, R. M., Xue, M., & Hung, S.-H. (2010). Slab-plume interaction
635 beneath the Pacific Northwest. *Geophys. Res. Lett.*, *37*(L14305). doi: 10.1029/
636 2010GL043489

637 Ogawa, M. (2003). Plate-like regime of a numerically modeled thermal convection in
638 a fluid with temperature-, pressure-, andstress-history-dependent viscosity. *J.*
639 *Geophys. Res.*, *108*(B2), 2067. doi: 10.1029/2000JB000069

640 Portner, D. E., Beck, S., Zandt, G., & Scire, A. (2017). The nature of subslab slow
641 velocity anomalies beneath south america. *Geophys. Res. Lett.*, *44*(10), 4747-
642 4755.

643 Portner, D. E., Rodríguez, E. E., Beck, S., Zandt, G., Scire, A., Rocha, M. P., ...
644 others (2020). Detailed structure of the subducted nazca slab into the lower
645 mantle derived from continent-scale teleseismic p wave tomography. *Journal of*
646 *Geophysical Research: Solid Earth*, *125*(5), e2019JB017884.

647 Pusok, A. E., & Stegman, D. R. (2020). The convergence history of India-
648 Eurasia records multiple subduction dynamics processes. *Science adv.*, *6*(19),
649 eaaz8681.

650 Rey, P. F., Coltice, N., & Flament, N. (2014). Spreading continents kick-started
651 plate tectonics. *Nature*, *513*, 405–408.

652 Ricard, Y., Richards, M. A., Lithgow-Bertelloni, C., & Le Stunff, Y. (1993). A geo-

dynamic model of mantle density heterogeneity. *J. Geophys. Res.*, *98*, 21895–21909.

Ruhl, M., Hesselbo, S. P., Jenkyns, H. C., Xu, W., Silva, R. L., Matthews, K. J., ... Riding, J. B. (2022). Reduced plate motion controlled timing of Early Jurassic Karoo-Ferrar large igneous province volcanism. *Science Advances*, *8*, eabo0866.

Stein, C., & Hansen, U. (2013). Arrhenius rheology versus Frank-Kamenetskii rheology–Implications for mantle dynamics. *Geochem., Geophys., Geosys.*, *14*, 2757–2770. doi: 10.1002/ggge.20158

Steinberger, B., & Calderwood, A. (2006). Models of large-scale viscous flow in the Earth's mantle with constraints from mineral physics and surface observations. *Geophys. J. Int.*, *167*, 1461–1481.

Sun, D., Miller, M. S., Holt, A. F., & Becker, T. W. (2014). Hot upwelling conduit beneath the Atlas Mountains, Morocco. *Geophys. Res. Lett.*, *41*, 8037–8044. doi: 10.1002/2014GL061884

Tackley, P. J. (2000a). Self-consistent generation of tectonic plates in time-dependent, three-dimensional mantle convection simulations 1. Pseudoplastic yielding. *Geochem., Geophys., Geosys.*, *1*(1021). doi: 10.1029/2000GC000036

Tackley, P. J. (2000b). Self-consistent generation of tectonic plates in time-dependent, three-dimensional mantle convection simulations 2. Strain weakening and asthenosphere. *Geochem., Geophys., Geosys.*, *1*(1026). doi: 10.1029/2000GC000043

Tan, E., Gurnis, M., & Han, L. (2002). Slabs in the lower mantle and their modulation of plume formation. *Geochem., Geophys., Geosys.*, *3*(1067). doi: 10.1029/2001GC000238

Tang, Y., Obayashi, M., Niu, F., Grand, S. P., Chen, Y. J., Kawakatsu, H., ... Ni, J. F. (2014). Changbaishan volcanism in northeast China linked to subduction-induced mantle upwelling. *Nature Geoscience*, *7*, 470–475.

Tao, K., Grand, S. P., & Niu, F. (2018). Seismic structure of the upper mantle beneath Eastern Asia from full waveform seismic tomography. *Geochem., Geophys., Geosys.*, *19*, 2732–2763.

Ueda, K., Gerya, T., & Sobolev, S. V. (2008). Subduction initiation by thermal–chemical plumes: numerical studies. *Phys. Earth Planet. Inter.*, *171*, 296–312.

van Heck, H., & Tackley, P. J. (2008). Planforms of self-consistently generated plate tectonics in 3-D spherical geometry. *Geophys. Res. Lett.*, *35*(L19312). doi: 10.1029/2008GL035190

van Hinsbergen, D. J. J., Steinberger, B., Doubrovine, P., & Gassmöller, R. (2011). Acceleration-deceleration cycles of India-Asia convergence: roles of mantle plumes and continental collision. *J. Geophys. Res.*, *116*(B06101). doi: 10.1029/2010JB008051

van Hinsbergen, D. J. J., Steinberger, B., Guilmette, C., Maffione, M., Gürer, D., Peters, K., ... others (2021). A record of plume-induced plate rotation triggering subduction initiation. , *14*, 626–630.

van Hunen, J., & van den Berg, A. P. (2008). Plate tectonics on the early Earth: limitations imposed by strength and buoyancy of subducted lithosphere. *Lithos*, *103*, 217-235.

Zhong, S. (2006). Constraints on thermochemical convection of the mantle from plume heat flux, plume excess temperature and upper mantle temperature. *J. Geophys. Res.*, *111*. doi: 10.1029/2005JB003972